INL/JOU-21-64894-Revision-0

The impact of anisotropic thermal expansion on the isothermal annealing of polycrystalline a-uranium

February 2022

Andrea M Jokisaari, Khadija Mahbuba, Yuhao Wang, Benjamin Beeler

Changing the World's Energy Future

INL is a U.S. Department of Energy National Laboratory operated by Battelle Energy Alliance, LLC

INL/JOU-21-64894-Revision-0

The impact of anisotropic thermal expansion on the isothermal annealing of polycrystalline a-uranium

Andrea M Jokisaari, Khadija Mahbuba, Yuhao Wang, Benjamin Beeler

February 2022

Idaho National Laboratory
Idaho Falls, Idaho 83415

http://www.inl.gov

Prepared for the
U.S. Department of Energy
Under DOE Idaho Operations Office
Contract DE-AC07-05ID14517

Computational Materials Science 205 (2022) 111217

Contents lists available at ScienceDirect

Computational Materials Science

journal homepage: www.elsevier.com/locate/commatsci

The impact of anisotropic thermal expansion on the isothermal annealing of polycrystalline α-uranium

Andrea M. Jokisaari [a,*], Khadija Mahbuba [b], Yuhao Wang [c], Benjamin Beeler [b]

[a] Computational Mechanics and Materials Department, Idaho National Laboratory, Idaho Falls, ID 83415, United States of America
[b] Nuclear Engineering Department, North Carolina State University, Raleigh, NC 27695, United States of America
[c] Nuclear Engineering and Radiological Sciences Department, University of Michigan, Ann Arbor, MI 48109, United States of America

ARTICLE INFO

Keywords:
Grain growth
Anisotropic thermal expansion
Uranium
Texture

ABSTRACT

Although grain growth impacts microstructural evolution in a wide variety of materials systems, the effect of anisotropic thermal expansion on grain boundary mobility and texture evolution has not been widely studied. Anisotropic thermal expansion occurs in multiple non-cubic metals, and the thermomechanical processing behavior of these materials can be better understood with further study into the impact of thermal expansion on grain boundary mobility and texture evolution. In this work, we develop a mesoscale phase field model of grain growth that includes the effect of anisotropic thermal expansion, which is applied to study polycrystalline α-uranium, a highly anisotropic metal. Three-dimensional simulations on polycrystalline α-uranium with and without thermal expansion eigenstrains are performed to study the grain boundary mobility and texture evolution as a function of temperature. A strain-free temperature of 933 K is selected, and the system is studied within the range of 873–933 K at intervals of ten degrees, resulting in increasing thermal eigenstrain with decreasing temperature. We also estimate a grain boundary mobility prefactor and activation energy based on existing experimental data of isothermal annealing of α-uranium. The grain boundary mobility is found to display significant deviation from Arrhenius behavior with the inclusion of thermal expansion eigenstrain as the amount of thermal eigenstrain (and thus elastic strain energy within the system) increases. This result explains an experimentally observed grain boundary mobility deviation from Arrhenius behavior. Furthermore, the texture evolution is affected, such that the grain orientations become less random with increasing thermal eigenstrain, which could explain experimentally observed texture behavior. These results indicate that the effect of thermal expansion should be considered when predicting the thermomechanical processing behavior of α-uranium and other materials with anisotropic thermal expansion.

1. Introduction

Anisotropic thermal expansion occurs in technologically relevant materials that exhibit non-cubic phases [1,2] (e.g., α-titanium, α-zirconium, zinc). Anisotropic thermal expansion causes different crystallographic directions of a single crystal to expand at different rates. Within the realm of non-cubic metals, the anisotropy is relatively weak, such that thermal expansion coefficients are typically positive but differ in magnitude. However, the orthorhombic α-uranium phase exhibits extremely anisotropic behavior, with the thermal expansion coefficient positive in the [100] and [001] crystallographic directions, but negative in the [010] direction [3,4].

Anisotropic thermal expansion has long been known to cause internal stresses high enough to induce plasticity within polycrystalline metallic materials. Cadmium, zinc, and tin cycled between cryogenic and room temperatures exhibit slip and twinning without grain growth [5]. However, there are relatively few detailed studies of the effect of anisotropic thermal expansion on other material behaviors, such as grain growth, recrystallization, or residual stresses affecting deformation. *In situ* heating X-ray diffraction experiments measured the evolution of residual strains in α-titanium polycrystals as a result of anisotropic thermal expansion [6], and a combination of experimental and computational work studied the elastoplastic response of the α-uranium system from thermal expansion. Elastoplastic self-consistent modeling of thermal stresses in polycrystalline α-uranium found stresses high enough to induce plastic flow, and neutron diffraction provided detailed information about slip and twinning modes [7]. Further studies examined the effect of residual thermal stresses on additional deformation [8,9]. In addition, a computational study using the phase field fracture method found that the negative coefficient of

* Corresponding author.
E-mail address: andrea.jokisaari@inl.gov (A.M. Jokisaari).

https://doi.org/10.1016/j.commatsci.2022.111217
Received 4 November 2021; Received in revised form 10 January 2022; Accepted 11 January 2022
Available online 1 February 2022

thermal expansion in α-uranium is capable of inducing plastic strains or fracture within polycrystalline α-uranium with a change in temperature of approximately 100 K from a stress-free state [10]. Finally, the effect of thermal expansion and surface energy on texture selection in copper thin films was studied with phase field modeling, though the study utilized only three grains with two orientations [11].

Conservative grain boundary motion, which entails only short-range atomic motion and no change in composition, is driven by differences in free energies on either side of the interface [12], and a major area of computational research focuses on curvature-driven grain growth. Atomistic studies, such as Ref. [12], provided a theoretical understanding of the role of grain boundary curvature on grain boundary motion and an Arrhenius relationship between grain boundary mobility and temperature. This Arrhenius relationship requires both a mobility prefactor and a thermal activation energy. At the mesoscale, the phase field method has become an extremely useful tool in modeling grain growth [13–15]. Early studies focused purely on curvature-driven grain growth, but advances in the mathematical model frameworks extended the capability to incorporate anisotropic grain boundary mobilities [16, 17]. Other contributions to the difference in free energy across an interface include elastic strain energy and defects [12]. The ability to incorporate elastic strain energy into phase field models provides a high-fidelity, spatially-resolved method to study its impact on grain growth. Phase field models have shown that an applied stress can affect grain texture evolution during annealing [18–21]. Strain energy from anisotropic thermal expansion or thermal expansion coefficient mismatches has also been suggested as a cause for abnormal grain growth [22]. Sometimes referred to as grain coarsening, abnormal grain growth results in certain grains becoming extremely large versus the overall grain population.

The phase field approach allows for the integration of multiphysics into a single simulation, providing a way to study the effect of anisotropic coefficients of thermal expansion on grain growth and texture evolution. Despite the evidence that anisotropic thermal expansion influences stresses within materials such as α-uranium, and that grain growth is affected by internal microstresses, detailed studies of the effect of anisotropic thermal expansion on grain growth are lacking. A thorough understanding of how anisotropic thermal expansion affects thermal microstresses, texture development, and grain growth during annealing and recrystallization is important for the development of novel alloys. This knowledge will aid in developing thermomechanical processing methods and in predicting their behavior during service in extreme thermal environments. The anisotropic thermal expansion of α-uranium will likely affect the grain boundary mobility and texture evolution during isothermal annealing.

In this work, we investigate the impact of anisotropic thermal expansion on grain growth and grain orientation (texture selection) in α-uranium using the phase field method. We calculate a mobility prefactor and activation energy based on experimental data. Additionally, we develop a phase field model of grain growth that includes the effect of anisotropic thermal expansion, and we perform three-dimensional simulations of grain growth with and without thermal expansion eigenstrain. One hundred grains with random orientations are used in each simulation and a total of 140 simulations are performed for statistical information. The grain boundary mobility as a function of temperature is calculated and inverse pole figures are used to study the evolution of the texture. We find that thermal eigenstrain accelerates the grain boundary mobility, with the deviation from the curvature-driven behavior increasing as the thermal eigenstrain increases. A similar type of behavior is observed in the experimental data. We also find that the texture becomes less random with increasing thermal eigenstrain. These results indicate that anisotropic thermal expansion can play a significant role in the thermomechanical processing and high-temperature behavior of α-uranium.

2. Phase field model

The phase field model in this work is based on the grain growth model in Ref. [17], with an additional energetic contribution from elastic strain energy similar to the work in Ref. [19]. Each grain, g, is represented by an order parameter, $\eta_g(\mathbf{r})$, where $\mathbf{r}$ indicates spatial position. Within a grain, η takes a value of one, while it takes a value of zero outside the grain, and its value smoothly varies between the two values within the diffuse grain boundary. Neighboring grains are represented by different η_g. Note that for ease of reading, the spatial dependence of the order parameter fields are not notated in the following equations, but the spatial dependence of other factors are notated. Similarly, the order parameter dependence of certain variables are not notated, but will become clear following the equations. The total free energy of the system is described as

$$\mathcal{F} = \int_V \left(f_0 + f_{\text{grad}} + f_{\text{el}} \right) dV, \tag{1}$$

where f_0 is the homogeneous free energy density, f_{grad} is the gradient energy density term related to the interfacial energy, and f_{el} accounts for elastic strain energy density arising from thermal expansion eigenstrains in the polycrystal. Following Ref. [17],

$$f_0\left(\eta_1, \eta_2, \ldots \eta_N\right) = A\left[\sum_{g=1}^{N}\left(\frac{\eta_g^4}{4} - \frac{\eta_g^2}{2}\right) + 1.5\sum_{g=1}^{N}\sum_{G>g}^{N}\eta_g^2\eta_G^2 + \frac{1}{4}\right], \tag{2}$$

where A is a parameter that affects the grain boundary energy. The expression f_0 is formulated such that the homogeneous energy is zero in the bulk. The gradient energy is defined as

$$f_{\text{grad}}\left(\eta_1, \eta_2, \ldots \eta_N\right) = \frac{\kappa}{2}\sum_{h=1}^{N}\left(\nabla\eta_g\right)^2, \tag{3}$$

where κ is the scalar gradient energy coefficient, which corresponds to an isotropic interfacial energy. Linear elasticity is chosen as the constitutive model relating stresses to strains. Using the Einstein summation convention, the elastic energy density contribution is described as

$$f_{\text{el}} = \frac{1}{2}C_{ijkl}(\mathbf{r})\epsilon_{ij}^{\text{el}}(\mathbf{r})\epsilon_{kl}^{\text{el}}(\mathbf{r}), \tag{4}$$

where C_{ijkl} is the local elastic stiffness tensor and $\epsilon_{ij}^{\text{el}}$ is the local elastic strain. The local elastic strain is described as

$$\epsilon_{ij}^{\text{el}}(\mathbf{r}) = \epsilon_{ij}^{\text{total}}(\mathbf{r}) - \epsilon_{ij}^{\text{TE}}(\mathbf{r}), \tag{5}$$

where $\epsilon_{ij}^{\text{TE}}(\mathbf{r})$ is the local thermal eigenstrain and the local total strain, $\epsilon_{ij}^{\text{total}}(\mathbf{r})$, is calculated as

$$\epsilon_{ij}^{\text{total}}(\mathbf{r}) = \frac{1}{2}\left[\frac{\partial u_i(\mathbf{r})}{\partial x_j} + \frac{\partial u_j(\mathbf{r})}{\partial x_i}\right], \tag{6}$$

and $u_i(\mathbf{r})$ is the displacement.

The temperature-dependent thermal eigenstrain is described following Ref. [10]. Each grain, g, has an associated unique orientation with respect to the reference frame of the computational domain that is described by a rotation tensor, R_{ij}^g. This rotation tensor can also be given by Euler angles that are transformed to a rotation tensor. Thus, the single-crystal values for the thermal eigenstrain tensor, $\epsilon_{ij}^{\text{TE}}$, and the elastic stiffness tensor, C_{ijkl}^{X}, must be rotated to represent their values for a given grain, such that

$$C_{ijkl}^g = R_{im}R_{jn}R_{ko}R_{lp}C_{mnop}^{\text{X}} \tag{7}$$

and

$$\epsilon_{ij}^{\text{TE},g} = R_{ik}R_{jl}\epsilon_{kl}^{\text{TE}}, \tag{8}$$

where C_{ijkl}^g is the rotated elastic stiffness tensor for the g^{th} grain and $\epsilon_{ij}^{\text{TE},g}$ is the rotated thermal eigenstrain tensor for the g^{th} grain. Note that $\epsilon_{ij}^{\text{TE}}$, C_{ijkl}^{X}, C_{ijkl}^g, and $\epsilon_{ij}^{\text{TE},g}$ are not spatial fields, merely single tensors. The thermal eigenstrain and elastic stiffness tensor at a given

point **r** within the material are defined by interpolating the tensors for each grain with the order parameters. The local thermal eigenstrain is defined as

$$\epsilon_{ij}^{\mathrm{TE}}(\mathbf{r}) = \frac{\sum_g \epsilon_{ij}^{\mathrm{TE},g} h(\eta_g)}{\sum_g h(\eta_g)}, \tag{9}$$

where

$$h(\eta_g) = \eta_g^3(6\eta_g^2 - 15\eta_g + 10) \tag{10}$$

is an interpolation function such that $h(0) = 0$ and $h(1) = 1$. The local elastic stiffness tensor is defined as

$$C_{ijkl}(\mathbf{r}) = \frac{\sum_g C_{ijkl}^g h(\eta_g)}{\sum_g h(\eta_g)}. \tag{11}$$

The stress at a point **r** in the material is determined by

$$\sigma_{ij}(\mathbf{r}) = C_{ijkl}(\mathbf{r})\epsilon_{kl}^{\mathrm{el}}(\mathbf{r}) \tag{12}$$

and the mechanical equilibrium equation is solved,

$$\nabla \cdot \sigma_{ij} = 0. \tag{13}$$

In this work, we use temperature-dependent values for the elastic stiffness of α-uranium from Ref. [23] and the anisotropic thermal expansion descriptions from Ref. [3].

The time evolution of the non-conserved order parameters is described with a set of Allen–Cahn equations [17],

$$\frac{\partial \eta_g}{\partial t} = -L\left[\frac{\partial f_0}{\partial \eta_g} + \frac{\partial f_{\mathrm{el}}}{\partial \eta_g} - \kappa\nabla^2\eta_g\right], \tag{14}$$

where L is the Allen–Cahn mobility, a property related to the grain boundary mobility [17], and t is the time. In this work, the scalar nature of L corresponds to an isotropic grain boundary mobility, which we assume given a lack of information to the contrary. The Arrhenius relationship for the mobility, M, is

$$M(T) = M_0 \exp\frac{-Q}{k_b T}, \tag{15}$$

where M_0 is the mobility prefactor, Q is the activation energy, k_b is the Boltzmann constant, and T is the temperature. The values for M_0 and Q are provided in Section 4, as they have been calculated for this work.

The phase-field model parameters are related to thermodynamic and kinetic parameters [17], with

$$A = \frac{3\gamma}{4l}, \tag{16}$$

$$\kappa = \frac{3}{4}\gamma l, \tag{17}$$

and

$$L = \frac{4M}{3l}, \tag{18}$$

where $l = 2$ μm is the diffuse interface width in the phase field model, and γ is the grain boundary energy. We use $\gamma = 0.79$ J/m^2 [24] as the average grain boundary energy. This work is focused specifically on the mechanistic effect of thermal eigenstrain, but future work studying grain growth in α-uranium could utilize anisotropic grain boundary energy.

3. Computational details and model limitations

The grain growth simulations are carried out using the Multiphysics Object Oriented Simulation Environment (MOOSE) [25]. The three-dimensional simulations are carried out with a domain size of (50 μm)^3. The simulations are meshed with (75 × 75 × 75) cubic, eight-node hexahedral elements, and linear Lagrange shape functions are used. The system of nonlinear equations is solved using the preconditioned Jacobian-free Newton–Krylov method with the BoomerAMG preconditioner from the *hypre* library [26]. Time integration is accomplished with the second backward differencing (BDF2) algorithm. To reduce computational cost, the GrainTracker algorithm [27] and adaptive time stepping are used. The grain structure is initialized via a random Voronoi tiling. Boundary conditions involve periodic boundaries on the order parameters, while the mechanical boundary conditions are designed to allow the domain to deform freely without any rigid body motion. On each coordinate axis, the plane that passes through the origin with its normal parallel to that axis has an applied Dirichlet boundary condition with zero displacements in the corresponding direction, while all other displacements are unconstrained.

Data analysis is performed with a combination of postprocessors internal to MOOSE and external Python libraries. The average grain diameter is calculated by using the MOOSE-based postprocessor that reports the average grain volume, $\bar{V}$, and assuming spherical grains. The grain boundary mobility is computed from the average squared diameter via the analytical relationship in Eq. (19). The slope of the linear fit of the average squared diameter versus time is then used to calculate the mobility. The linear fit of the average squared diameter data is performed using the Python scikit-learn library [28] over the interval of 95 grains to 20 grains, and the justification for that interval is given in Section 4.2.1. Inverse pole figures are plotted using the Python library pymicro [29] to visualize the grain orientations.

This phase field model breaks down when the elastic strain energy is large enough. The strain energy induced in the system can be so large locally that it is energetically favorable to develop new non-zero order parameter values within a grain to reduce the local eigenstrain value (Eq. (9)). The reduction in the associated elastic energy of the system due to spurious phase formation can overcome the increased penalty of gradient and barrier energies. In the α-uranium system, a change of approximately 40–50 K can result in local stresses on the order of 500 MPa, which is well above the reported uniaxial yield strength for α-uranium at 873 K [30]. The phase field model assumes pure linear elastic behavior and does not account for the plastic flow that would occur at high stresses, providing a physical limitation to the range of temperatures that can be studied. We find that the phase field model breaks down due to large elastic energies at around 873–883 K, or more specifically, with a deviation of approximately 40–50 K from the strain-free temperature. The temperature range of the investigation is chosen such that the simulations stay within 50 K of the strain-free temperature. Thus, model breakdown occurs when plastic behavior should occur, which does not place additional constraints on the range of temperatures that can be studied.

4. Results and discussion

The effect of thermal eigenstrain on grain growth in a polycrystalline material is investigated for the α-uranium system by performing novel phase field simulations and comparing to existing experimental data. A grain boundary mobility for α-uranium is estimated from isothermal annealing data in the literature. The estimated mobility is then used within phase field simulations to study the effect of thermal eigenstrain on grain boundary motion and grain coarsening. Before presenting the results of the grain growth model with the addition of thermal eigenstrain, the system behavior without thermal eigenstrain is first discussed. The results are placed in the context of existing experimental data on thermal processing of α-uranium.

4.1. Grain boundary mobility

The experimental data in Ref. [31] for α-uranium grain growth versus time during isothermal annealing are used to estimate a grain boundary mobility based on an Arrhenius relationship. These are the only experimental data available to date within the literature that

directly measure grain growth as a function of time at different temperatures for α-uranium. In Ref. [31], multiple swaging and annealing steps were performed to reduce the initial grain size of the material. Three different sample groups were created by changing the penultimate sample annealing procedures, and samples were annealed for grain growth measurements at 823 K, 873 K, 898 K, and 923 K, though not all temperatures were studied for all groups. We note that the mobility calculated from these experimental data is by no means definitive, but is principally used to provide a reasonable value for the phase field model. The data show rapid initial grain growth, then almost-stalled grain growth. Ref. [31] indicates that carbon and silicon impurities form precipitates that slow grain growth in α-uranium. The initial rapid grain growth likely represents the true grain boundary mobility due to the high driving forces at small grain sizes, while the slower or stalled grain growth at longer times is likely the result of grain boundary pinning by impurities and precipitates [32]. Thus, the initial grain growth data for the first hour of reported annealing data are used to compute grain boundary mobility according to [15]

$$\bar{D}^2(t) = \bar{D}_0^2 + \frac{1}{2}\alpha\gamma M t, \tag{19}$$

where $\bar{D}(t)$ is the average grain diameter as a function of time, $\bar{D}_0$ is the initial average grain diameter, and α is a dimensional factor equal to 0.5 in three dimensions. The values of $\bar{D}_0$ and $\bar{D}(t)$ are provided in the data, a linear fit to the equation is performed, and the equation is solved for M. To reduce the impact of possible precipitates on the calculated grain boundary mobility, only the grain growth data from 923 K and 898 K are used. The mobility values calculated for two groups are similar, but the values for the third group are significantly lower. Given the sample preparation [31], the third group likely has more precipitates than the other two groups, and thus, the mobility from the third data is excluded and the values for the first two groups are used. Values of $M_0 = 1.85 \times 10^{-8}$ m^4/J s and $Q = 1.07$ eV are found.

4.2. Phase field simulations of grain growth

A series of three-dimensional phase field simulations are used to investigate the effect of thermal eigenstrain on grain growth in polycrystalline α-uranium. Two broad classes of conditions are studied: grain growth without thermal eigenstrain as a baseline for comparison, and grain growth with thermal eigenstrain. The simulations are designed to approximate the isothermal annealing behavior of a cast material cooled through the α/β phase boundary that formed small α-phase grains, then was annealed at a target temperature. The strain-free temperature (i.e., the temperature at which the thermal eigenstrain is zero), is chosen as 933 K, near the α/β phase boundary of 941 K [33]. Grain growth behavior is investigated at 933 K, 923 K, 913 K, 903 K, 893 K, 883 K, and 873 K. One hundred grains are initially represented within the computational domain with random Euler rotation angles. Ten initial grain structures, with their associated grain orientations, are investigated for each temperature with and without thermal eigenstrain, for a total of 140 simulations.

4.2.1. Without thermal expansion strains

The behavior of the grain growth simulations without thermal eigenstrain is first examined to understand the evolution in the number of grains, average grain size, and grain orientation. As an example, Fig. 1 shows the evolution of the total free energy, average grain volume, and total number of grains present in a simulation without thermal eigenstrain at 903 K. The light blue lines on each plot indicate the time at which 95 grains (left line) and 20 grains (right line) exist. There is a brief period of grain boundary motion and relaxation from the initial Voronoi grain construction as the grain structure becomes equiaxed, as evidenced by the steep initial drop in system energy and almost constant number of grains. After this initial relaxation, which occurs typically with the loss of two grains, grain growth proceeds and the number of grains and average grain size vary rapidly with time, until approximately fifteen grains remain. At this point, the changes in the number of grains and the average grain volume become obviously discrete with long times between changes in values. Boundary effects become significant with the further loss of grains, resulting in the loss of bulk behavior. As a result, the data are sampled over the range of 95 to 20 grains to capture bulk behavior during grain growth and avoid initial condition and domain boundary effects. In other words, the interval of 95 to 20 grains provides the largest consistent interval of normal grain growth behavior over which to sample. In addition, Fig. 1(d) presents the average of the grain diameter squared ($\bar{D}^2$) assuming spherical grains. The linear fit over the interval of 95 to 20 grains is shown with the dashed red line, which samples the linear region of the data. When actually implementing Eq. (19), the time at the first instance of 95 grains is taken as the new initial time of zero (i.e., the average grain diameter at this time is taken as $\bar{D}_0$). The linear fit agrees well with the plot of $\bar{D}^2(t)$.

Finally, we compare grain orientations versus time. Each grain has a unique identity within the simulation, which is tied to a unique Euler angle describing the grain rotation with respect to the simulation axes. This identification is used to determine which grains disappear and in what order. For the systems without thermal strain, the grain orientations for each of the ten cases evolve the same way regardless of the temperature, as expected for a system without any thermally varying anisotropic properties. An example of the grain orientation for a system at 903 K without thermal strain is plotted in Fig. 2. The grain orientations of the initial grain structure, and for 70 and 27 remaining grains, are presented in inverse pole figures for the z-direction of the computational domain. Grains do not rotate during grain growth, but the overall sample texture may change due to disappearance of certain grains. The initial grain orientations are scattered over a wide range, and the random grain orientations are retained throughout the process of grain growth as evinced by grains with orientations near each of the {100}, {101}, and {111}. Due to the orthorhombic crystal structure of α-uranium, (100) is crystallographically different from (010), etc., but for brevity, all of the possibilities will not be listed, and the listed directions will be used as a shorthand.

The mobility results indicate that the phase field simulations accurately capture grain growth behavior without thermal eigenstrain, providing a basis for comparison of the results with thermal eigenstrain. Fig. 3(a) presents a box-and-whisker plot of mobility as a function of temperature from the phase field simulations without thermal eigenstrain, including the median value at each temperature and the spread of the values at each temperature. The whiskers represent 1.5 times the interquartile range. As expected, there is minor scatter of the calculated mobility due to the different grain structures, and the variation increases with increasing temperature. Fig. 3(b) presents the logarithm of the mobility versus the inverse temperature for the analytically calculated value and the average phase field mobility at each temperature. When plotting the logarithm of the mobility versus the inverse temperature, an Arrhenius relationship will result in a straight line in which the slope corresponds to the activation energy and the vertical offset is related to the mobility prefactor. The average mobility from the phase field simulations is found to retain the same slope as the analytical calculation, indicating a minor difference in the mobility prefactor, though the activation energy is not affected. This small deviation is likely due to the presence of the diffuse interface in the phase field model [17].

4.2.2. With thermal expansion strains

Next, the grain growth behavior of the system is investigated with the influence of thermal eigenstrain. Fig. 4 shows a cross-section of the computational domain during grain growth with thermal eigenstrain at 903 K with 60 remaining grains, illustrating both the grain structure and the elastic energy density. The example presented here with thermal eigenstrain has the same initial grain structure and grain

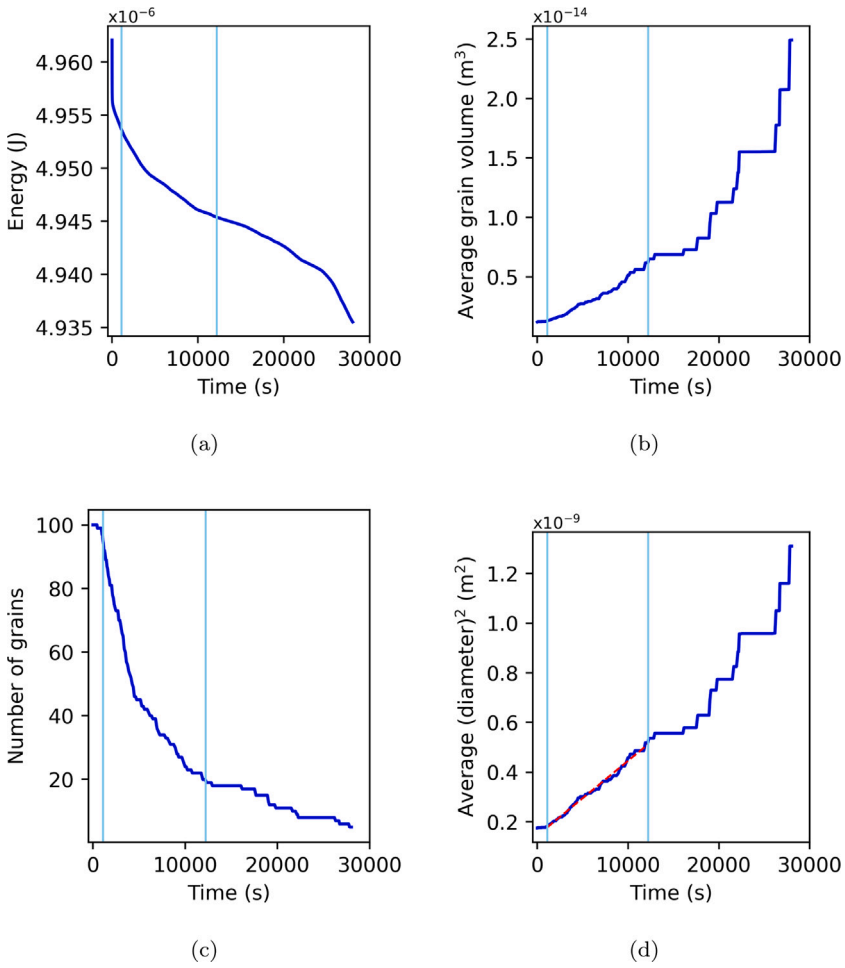

Fig. 1. The evolution of the (a) total free energy, (b) average grain volume, (c) number of grains, and (d) the average squared diameter versus time for an α-uranium system without thermal eigenstrain at 903 K. In (d), the linear fit to the data is shown with the dashed red line between the two light blue vertical lines. The data are presented from 100 to five grains, and the two light blue lines in each plot indicate the times at which 95 and 20 grains exist. There is rapid initial relaxation of the system and discretization of the average grain volume at long simulation times.

orientation as for the results presented in Figs. 1, 1(d), and 2. The time evolution of the number of grains, average grain size, total free energy, and average squared grain diameter are presented in Fig. 5. We again sample over the interval of 95 to 20 grains, which remains a large, consistent interval of normal grain growth behavior over which to sample. Similar behavior is observed compared to the case without thermal eigenstrain, such as the initial relaxation period of the Voronoi grain structure, but the kinetics are accelerated. The decrease in the number of grains proceeds at a similar rate for the cases with and without thermal eigenstrain until approximately 50 grains remain. The rate then slows for the system without thermal eigenstrain, while losing grains at the same rate for the system with thermal eigenstrain. This difference is also reflected in the shape of the curve for the average squared grain diameter. The average squared diameter versus time is approximately linear without thermal eigenstrain, but a deviation from linear behavior is observed at later times with the presence of thermal eigenstrain.

The inverse pole figures in Fig. 7 indicate that the specific grain orientations that disappear are impacted by the presence of thermal strain. The inverse pole figure for the initial grain configuration is the same as that presented in Fig. 2. However, the grains that disappear differ between the two simulations. Although the inverse pole figures are not snapshots of the structures with identical numbers of grains, they are at similar points of the evolution (i.e., 70 grains versus 60 grains for the middle portion of the grain growth, and 27 versus 23 grains for the late stage). Because the grains do not rotate, but rather only disappear, the specific orientations may be compared. If the pattern of grain disappearance is identical, then all the orientations present for inverse pole figures with the fewer number of grains would be present in the inverse pole figures with the larger number of grains. However, orientations are present in the inverse pole figures for the simulations with thermal eigenstrain at the middle and late stages of grain growth that are not present at the middle and late stages for the simulations without thermal eigenstrain. Thus, the exact grains that disappear during grain growth are affected by the presence of thermal eigenstrain in the polycrystalline material. Specifically, Fig. 6(c) shows that most of the remaining grains in the z-axis of the sample are near the {001}, {101}, and {100} orientations, with virtually no grains near the {111} and {010} orientations, unlike the case without thermal eigenstrain. The α-uranium crystal has a positive coefficient of thermal expansion in the [100] and [001] directions and a negative coefficient in the [010] direction. As a result, favorably oriented grains with low elastic strain energy will preferentially grow at the expense of unfavorably oriented grains. As grain growth proceeds and the number of remaining grains decreases, a preferential orientation will arise for the remaining grains. Although the exact preferential orientation is likely to vary depending on the initial grain orientations and morphologies, some preferential orientation will always arise. No conclusion can be drawn about high-energy or low-energy grain orientations, however, because the degree of misorientation between grains drives elastic energy. Furthermore, the degree of randomness decreases in the orientation of the grains at the later stage of grain growth as the amount of thermal eigenstrain

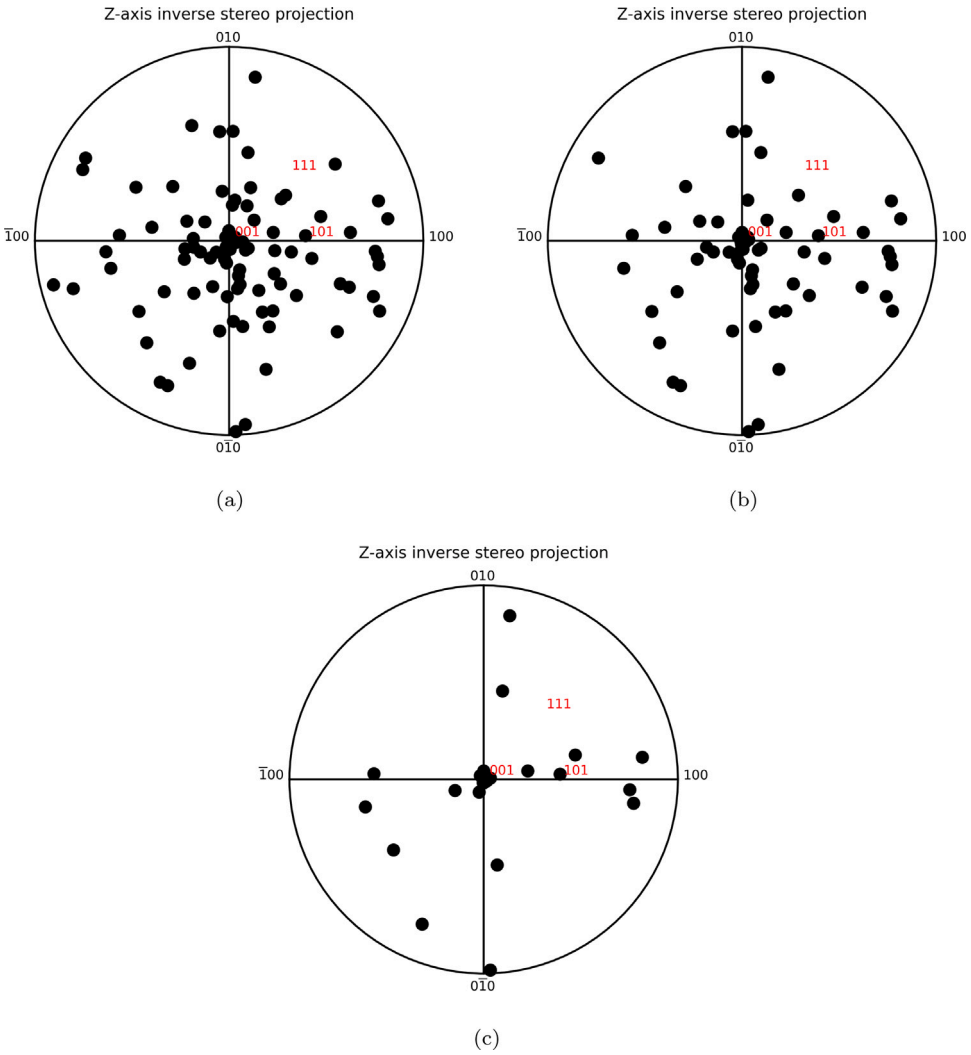

Fig. 2. Inverse pole figures for the z-direction of the computational domain illustrating the orientation of the remaining grains during grain growth for a simulation without thermal eigenstrain at 903 K. (a) Initial condition with 100 grains, (b) 70 grains remaining, (c) 27 grains remaining. Grains do not rotate during grain growth but the overall sample texture may change due to disappearance of certain grains.

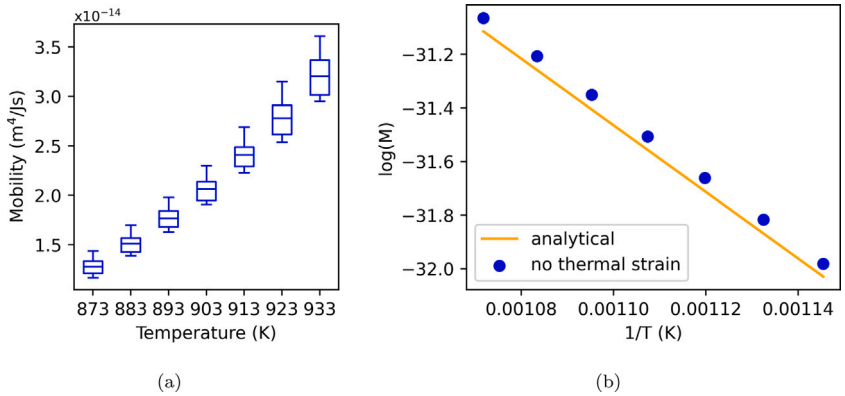

Fig. 3. The calculated mobility versus temperature for the grain growth simulations of α-uranium without thermal eigenstrain. (a) Box-and-whisker plot indicating the median and spread of the values, with each whisker equal to 1.5 times the interquartile range, (b) logarithm of the mobility versus the inverse temperature for the analytical calculation as well as the results from the phase field simulations. The variation in mobility increases as temperature increases, while the average mobility values—as calculated by the phase field simulations—are slightly larger than the analytical values. The activation energy is not affected, but the mobility prefactor may be slightly affected in the phase field simulations.

increases (i.e., as the temperature decreases), as seen in Fig. 7. At 933 K, the inverse pole figure indicates grains oriented in many directions, with a progressive clustering of the grain directions as temperature decreases. This kind of behavior is observed in other instances of the simulations of grain growth with thermal eigenstrain. Texture evolution is reported after thermal processing of α-uranium [34,35]. This result indicates that thermal eigenstrain could play a significant role in this texture evolution process.

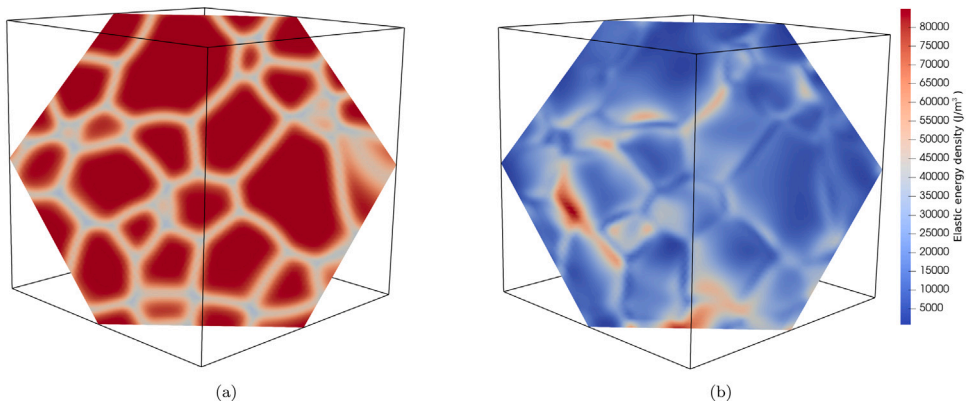

Fig. 4. A cross-section of the computational domain during grain growth with thermal eigenstrain at 903 K, sixty grains remaining. (a) The grain structure, and (b) the elastic strain energy density. The elastic energy density is heterogeneous throughout the grain structure and even within individual grains.

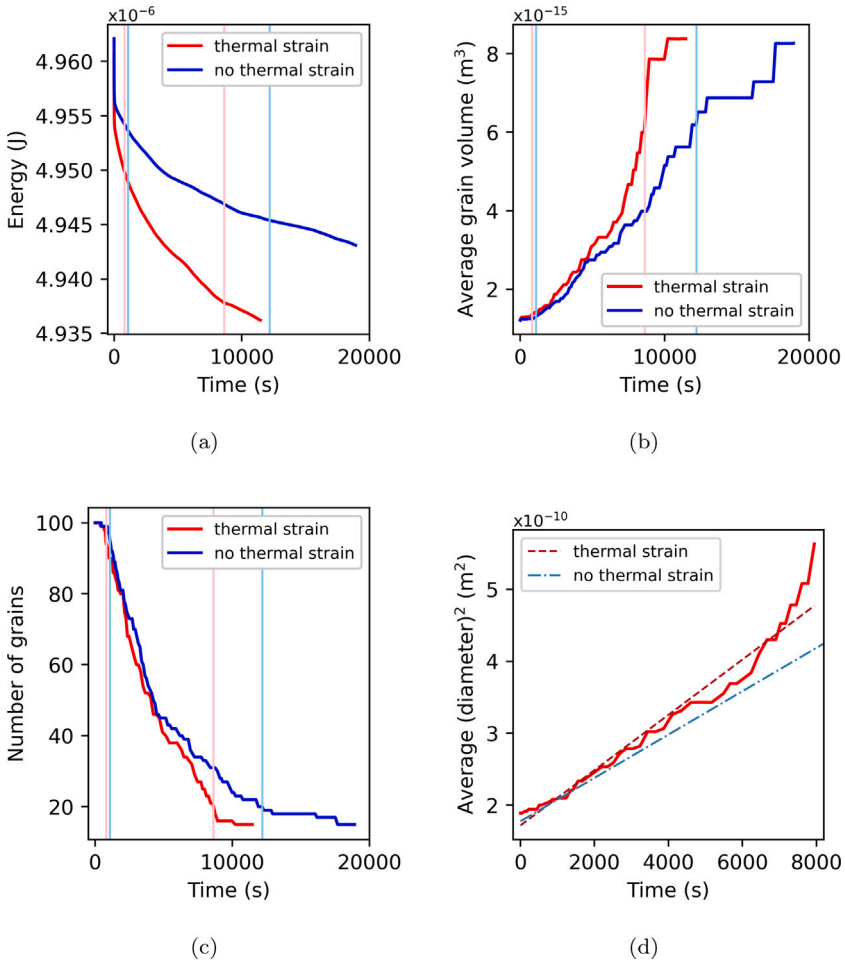

Fig. 5. The evolution of the (a) total free energy, (b) average grain volume, (c) number of grains, and (d) average squared grain diameter versus time for an α-uranium system from 100 to 15 grains at 903 K. The system with thermal eigenstrain is in blue, while the data for the same system without thermal eigenstrain (Fig. 1) is shown in red. The vertical lines show the times at which 95 and 20 grains exist (light blue for the system without thermal strain, pink for the system with thermal strain). The same initial relaxation period of the Voronoi initial grain structure is evident, followed by grain growth. Note that in (d) the time axis is shifted and truncated to the range of 95 to 20 grains only for the system with thermal eigenstrain. The linear fit to the thermal eigenstrain data is shown in red, while the linear fit for the system without thermal eigenstrain is reproduced for comparison.

The disappearance of specific grains within polycrystalline α-uranium is affected by the presence of thermal strain. As mentioned previously, the pattern of grain disappearance (texture evolution) for a system without thermal strain evolves the same way regardless of temperature, which is expected due to the isotropic grain boundary energy and no anisotropic, thermally dependent properties. When thermal strain is present, the specific grains that disappear vary depending on the temperature. At 933 K, for which the thermal strain is 0, the texture evolution is the same between both cases. As the temperature decreases and the amount of thermal eigenstrain increases, different

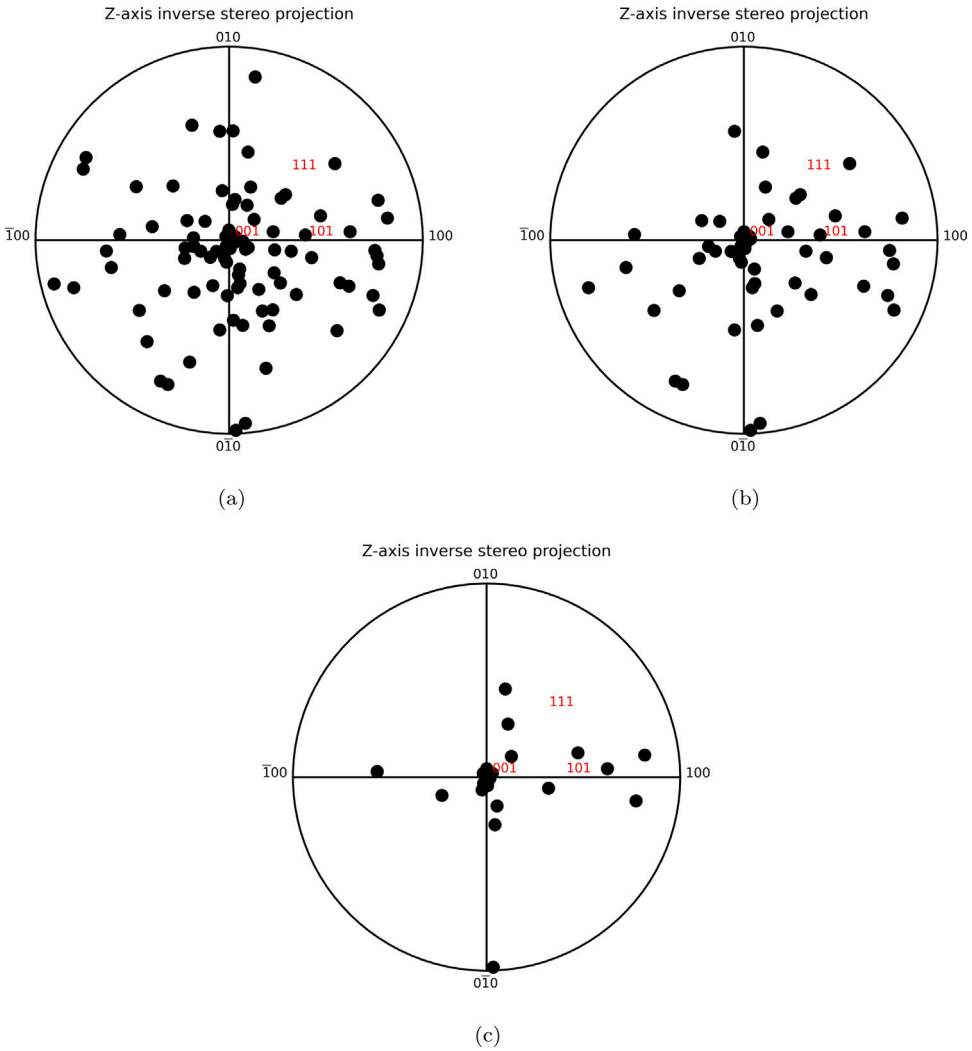

Fig. 6. Inverse pole figures for the z-direction of the computational domain illustrating the orientation of the remaining grains during grain growth for a simulation with thermal eigenstrain at 903 K. (a) Initial condition with 100 grains, (b) 60 grains remaining, and (c) 23 grains remaining. Grains do not rotate during grain growth but the overall sample texture may change due to disappearance of certain grains.

grains disappear; the variation in grain disappearance increases with increasing eigenstrain (Fig. 7). This is due to the increase in elastic strain energy in the system with decreasing temperature (i.e., a larger change in temperature from the strain-free temperature). The elastic strain energy density varies locally, with some grains having a lower elastic strain energy than others dependent upon the specific configuration of grain morphologies and orientations. A higher elastic strain energy retards grain growth, such that a fast-growing grain will be slowed or a slow-growing grain will be consumed by another growing grain [18].

The mobility of the system with thermal eigenstrain displays the same qualitative behavior as the mobility calculated from the experimental data. The mobilities obtained from the phase field simulations with and without thermal eigenstrain are presented in Fig. 8. The calculated mobilities are not statistically different at 933 K, but the results diverge with decreasing temperature (i.e., increasing thermal eigenstrain) so mobility is larger with the presence of thermal eigenstrain in the polycrystalline material. There are two outlier values for the mobility with thermal eigenstrain at 883 K. These outliers are determined as being more than three standard deviations from the average in the 883 K data set. The outlier values are a result of a model breakdown which occurred when stress-free grains nucleated and grew at the expense of the strained grains. It is possible the model breakdown also occurred at 893 K given some of the computed mobility values are within the range of the results without thermal eigenstrain. Another source of scatter in the mobility data for the simulations with thermal eigenstrain is the linear fitting procedure for calculating the mobility. As described previously, the average squared grain diameter behavior can deviate from linear behavior in the systems with thermal eigenstrain. An additional presentation of the data in the form of the logarithm of the mobility versus the inverse temperature is presented in Fig. 9. The mobility with thermal eigenstrain is the same as the mobility without thermal strain at 933 K. This is to be expected, as the strain-free temperature is 933 K. At lower temperatures, the mobility with thermal strain is greater than the mobility without thermal strain, and the difference between the values at each temperature increases as the temperature decreases. The average mobility at 883 K with thermal strain is actually greater than the mobility at 893 K because of the larger strain energy at 883 K. There is more scatter in the calculated mobility at each temperature when thermal strain is included due to the different initial grain orientations since elastic energy varies with different initial conditions.

The mobility calculated from the phase field simulations with the addition of thermal eigenstrain displays an evident effect of elastic strain energy increasing the mobility at lower temperatures than would arise from a pure Arrhenius relationship. Interestingly, the experimental data in Ref. [31] displays a similar deviation from an Arrhenius relationship, though due to the small sample size, any conclusions

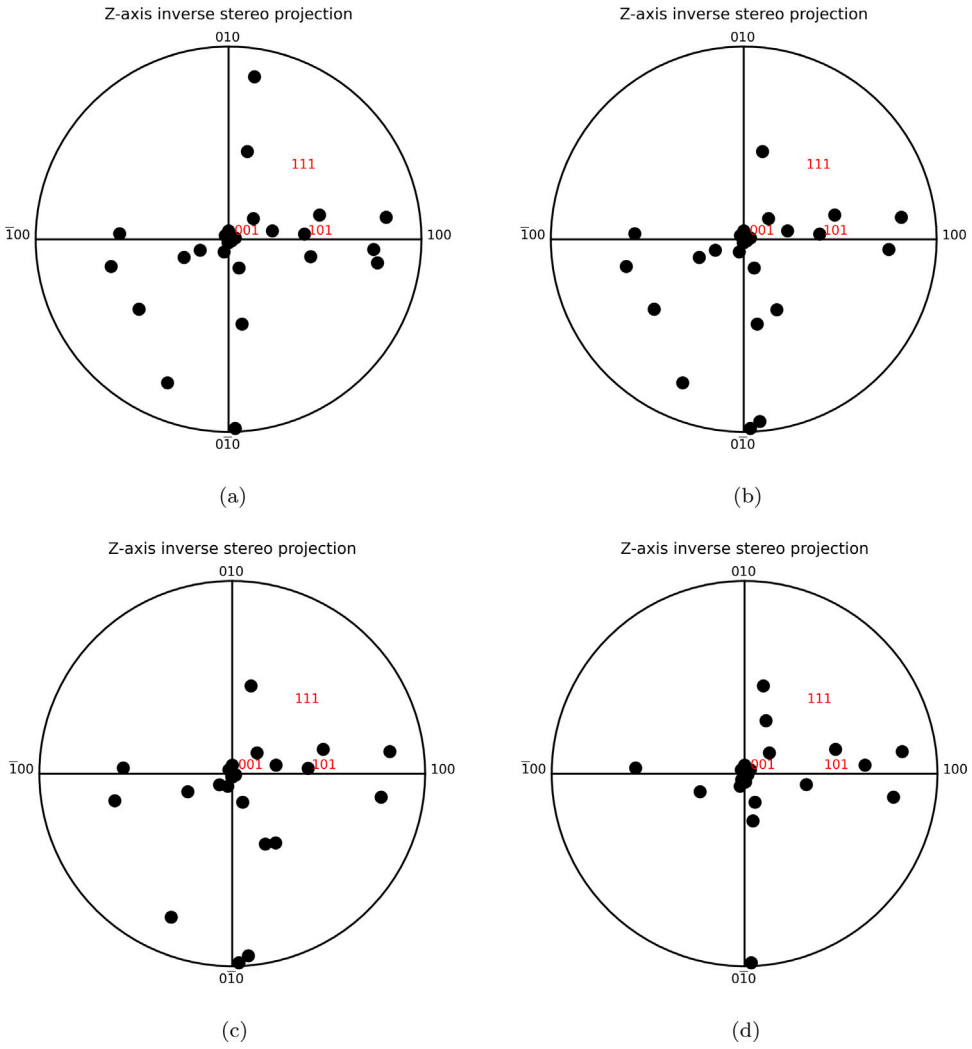

Fig. 7. Inverse pole figures for the z-direction of the computational domain illustrating the orientation of the remaining grains during grain growth for a simulation with thermal eigenstrain at (a) 933 K, for which the eigenstrain is 0 with 30 grains (b) 923 K with 30 grains, (c) 913 K with 27 grains, and (d) 903 K with 23 grains. The thermal eigenstrain increases with decreasing temperature, and the grain orientations become less random with increasing thermal eigenstrain.

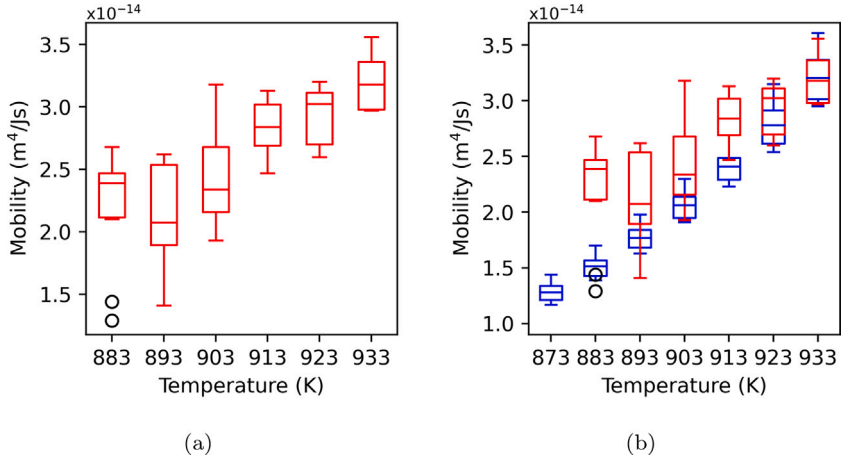

Fig. 8. Box plots of the mobility calculated from the phase field simulations (a) with thermal eigenstrain and (b) an overlay of the data with and without thermal eigenstrain. Red indicates simulations with thermal eigenstrain and blue indicates simulations without thermal eigenstrain. Black circles are outlier data points for simulations with thermal eigenstrain. The calculated mobilities are not statistically different at 933 K, but the results diverge with decreasing temperature (i.e., increasing thermal eigenstrain) so the mobility is larger with the presence of thermal eigenstrain in the polycrystalline material. There are two outliers for the mobility with thermal eigenstrain at 883 K, which lie within the range of the data without thermal eigenstrain. These are a result of the model breakdown.

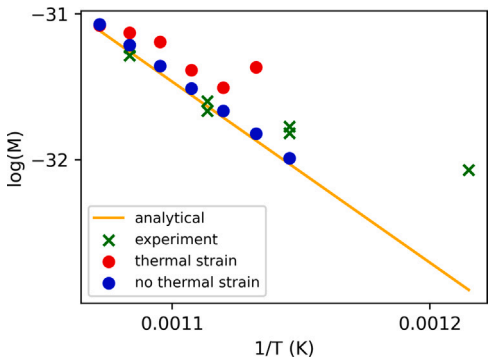

Fig. 9. Logarithm of the mobility versus the inverse temperature for the values obtained from the phase field simulations with and without thermal eigenstrain, as well as the for the experimental data from Ref. [31], and the analytical mobility as predicted by an Arrhenius relationship. The mobility obtained from the phase field simulations is the same for the two cases at the lowest inverse temperature at which the thermal eigenstrain is zero, and at lower temperatures, the mobility for the system with thermal eigenstrain is greater than the system without it. The uptick in the mobility at 883 K with thermal eigenstrain is a result of the very large elastic driving force. The mobility obtained from the experimental data has a qualitatively similar relationship to the phase field mobility with thermal eigenstrain, diverging significantly from the analytical mobility and phase field mobility calculated without thermal eigenstrain..

drawn must be tentative and will require further experimental work to confirm. As shown in Fig. 9, with decreasing temperature there is a progressive deviation of mobility values measured from the grain growth data versus the mobility values from an Arrhenius relationship. The values computed from the grain growth data are larger at lower temperatures than the values that would result from an Arrhenius relationship. However, the deviation occurs over a larger temperature difference (down to 823 K) than occurs with the phase field simulations. The experimental grain growth data were gathered from specimens that had undergone several swaging and annealing procedures to generate an equiaxed and small (10 μm) grain structure. Recrystallization annealing steps started at 873 K, causing partial recrystallization, and proceeded at lower temperatures to recrystallize more of the material. This thermal processing technique would result in a material comprised of grains with different stress-free strain temperatures that are above the isothermal annealing temperature. The experimental mobility may display this deviation from Arrhenius behavior as a result of this spectrum of stress-free strain temperatures.

5. Conclusions

In this work, a model is presented to study the effect of anisotropic thermal expansion on grain growth in polycrystalline α-uranium. Although anisotropic thermal expansion occurs in multiple non-cubic metals, to date the phenomenon has not been widely studied. The phase field approach is used to predict the impact of thermal eigenstrain arising from anisotropic thermal expansion in the polycrystalline material on grain boundary mobility and grain texture selection during isothermal annealing. We study the behavior of α-uranium without thermal eigenstrain as a basis for comparison and find that the thermal eigenstrains can significantly influence both the grain boundary mobility and the texture selection if the temperature varies by approximately 30 K from the strain-free temperature. We also extract grain boundary mobility information from experimental grain growth data and find that the experimental grain boundary mobility deviates from Arrhenius behavior in a qualitatively similar manner as that observed in the simulations. This work indicates that several things should be considered when dealing with α-uranium in particular and other materials with anisotropic coefficients of thermal expansion in general. First and most broadly, the effect of thermal expansion should be considered when predicting the results of thermomechanical processing of α-uranium, even when relatively small temperature deviations from a strain-free temperature occur (e.g., the temperature at which a material recrystallized). Second, the thermal eigenstrains could drive rapid grain boundary motion. Third, texture selection during annealing may naturally arise and be difficult to remove during recrystallization, as internal stresses may select the preferential growth of favorably oriented nuclei. An experimental annealing study on α-uranium in which the initial microstructure is generated with a stress-free temperature near the α phase boundary would confirm or invalidate the grain boundary mobility predictions in this work. A possible material synthesis method would be to sinter high-purity α-uranium powder at 930 K.

CRediT authorship contribution statement

Andrea M. Jokisaari: Conceptualization, Methodology, Software, Investigation, Writing – original draft, Writing – review & editing, visualization. **Khadija Mahbuba:** Investigation, Writing – review & editing. **Yuhao Wang:** Investigation, Writing – review & editing. **Benjamin Beeler:** Conceptualization, Writing – review & editing.

Declaration of competing interest

The authors declare that they have no known competing financial interests or personal relationships that could have appeared to influence the work reported in this paper.

Data availability statement

The raw/processed data required to reproduce these findings cannot be shared at this time due to legalreasons.

Acknowledgments

The author gratefully acknowledges that this work is supported through the Laboratory Directed Research and Development (LDRD) program at Idaho National Laboratory (INL) under DOE Idaho Operations Office Contract DE-AC07-05ID14517. This manuscript has been authored by Battelle Energy Alliance, LLC under the aforementioned contract, and the High Performance Computing center at INL is also supported under the same contract number. The United States Government retains and the publisher, by accepting the article for publication, acknowledges that the United States Government retains a nonexclusive, paid-up, irrevocable, world-wide license to publish or reproduce the published form of this manuscript, or allow others to do so, for United States Government purposes.

References

[1] B. Childs, The thermal expansion of anisotropic metals, Rev. Mod. Phys. 25 (3) (1953) 665.
[2] R. Meyerhoff, J. Smith, Anisotropic thermal expansion of single crystals of thallium, yttrium, beryllium, and zinc at low temperatures, J. Appl. Phys. 33 (1) (1962) 219–224.
[3] L.T. Lloyd, C. Barrett, Thermal expansion of alpha uranium, J. Nucl. Mater. 18 (1) (1966) 55–59.
[4] B. Beeler, K. Mahbuba, Y. Wang, A. Jokisaari, Determination of thermal expansion, defect formation energy, and defect-induced strain of α-U via ab initio molecular dynamics, Front. Mater. 8 (2021) 188.
[5] W. Boas, R.W.K. Honeycombe, The anisotropy of thermal expansion as a cause of deformation in metals and alloys, Proc. R. Soc. A 188 (1015) (1947) 427–439.
[6] Z. Zheng, P. Eisenlohr, T. Bieler, D.C. Pagan, F.P. Dunne, Heterogeneous internal strain evolution in commercial purity titanium due to anisotropic coefficients of thermal expansion, JOM 72 (1) (2020) 39–47.
[7] C. Calhoun, J. Wollmershauser, D. Brown, R. Mulay, E. Garlea, S. Agnew, Thermal residual strains in depleted α-U, Scr. Mater. 69 (8) (2013) 566–569.
[8] C. Calhoun, E. Garlea, R. Mulay, T. Sisneros, S. Agnew, Investigation of the effect of thermal residual stresses on deformation of α-uranium through neutron diffraction measurements and crystal plasticity modeling, Acta Mater. 85 (2015) 168–179.

[9] C. Calhoun, E. Garlea, T. Sisneros, S. Agnew, In-situ neutron diffraction characterization of temperature dependence deformation in α-uranium, J. Nucl. Mater. 502 (2018) 60–67.
[10] A.A. Rezwan, A.M. Jokisaari, M.R. Tonks, Modeling brittle fracture due to anisotropic thermal expansion in polycrystalline materials, Comput. Mater. Sci. 194 (2021) 110407.
[11] M. Jamshidian, P. Thamburaja, T. Rabczuk, Modeling the effect of surface energy on stressed grain growth in cubic polycrystalline bodies, Scr. Mater. 113 (2016) 209–213.
[12] M. Upmanyu, R. Smith, D.J. Srolovitz, Atomistic simulation of curvature driven grain boundary migration, Interface Sci. 6 (1) (1998) 41–58.
[13] D. Fan, L.-Q. Chen, Computer simulation of grain growth using a continuum field model, Acta Mater. 45 (2) (1997) 611–622.
[14] I. Steinbach, F. Pezzolla, B. Nestler, M. Seeßelberg, R. Prieler, G.J. Schmitz, J.L. Rezende, A phase field concept for multiphase systems, Physica D 94 (3) (1996) 135–147.
[15] N. Moelans, F. Wendler, B. Nestler, Comparative study of two phase-field models for grain growth, Comput. Mater. Sci. 46 (2) (2009) 479–490.
[16] B. Nestler, A.A. Wheeler, Anisotropic multi-phase-field model: Interfaces and junctions, Phys. Rev. E 57 (3) (1998) 2602.
[17] N. Moelans, B. Blanpain, P. Wollants, Quantitative phase-field approach for simulating grain growth in anisotropic systems with arbitrary inclination and misorientation dependence, Phys. Rev. Lett. 101 (2) (2008) 025502.
[18] D.-U. Kim, S.G. Kim, W.T. Kim, J. Cho, H.N. Han, P.-R. Cha, Effect of microelasticity on grain growth: Texture evolution and abnormal grain growth, Scr. Mater. 64 (12) (2011) 1079–1082.
[19] M. Tonks, P. Millett, Phase field simulations of elastic deformation-driven grain growth in 2D copper polycrystals, Mater. Sci. Eng. A 528 (12) (2011) 4086–4091.
[20] S. Bhattacharyya, T.W. Heo, K. Chang, L.-Q. Chen, A phase-field model of stress effect on grain boundary migration, Modelling Simul. Mater. Sci. Eng. 19 (3) (2011) 035002.
[21] E. Shahnooshi, M. Jamshidian, M. Jafari, S. Ziaei-Rad, T. Rabczuk, Phase field modeling of stressed grain growth: Effect of inclination and misorientation dependence of grain boundary energy, J. Cryst. Growth 518 (2019) 18–29.
[22] E.M. Zielinski, R. Vinci, J. Bravman, The influence of strain energy on abnormal grain growth in copper thin films, Appl. Phys. Lett. 67 (8) (1995) 1078–1080.
[23] E. Fisher, Temperature dependence of the elastic moduli in alpha uranium single crystals, part IV (298 to 923 K), J. Nucl. Mater. 18 (1) (1966) 39–54.
[24] K. Mahbuba, B. Beeler, A. Jokisaari, Evaluation of the anisotropic grain boundaries and surfaces of α-U via molecular dynamics, J. Nucl. Mater. (2021) 153072.
[25] C.J. Permann, D.R. Gaston, D. Andrš, R.W. Carlsen, F. Kong, A.D. Lindsay, J.M. Miller, J.W. Peterson, A.E. Slaughter, R.H. Stogner, et al., MOOSE: Enabling Massively parallel multiphysics simulation, SoftwareX 11 (2020) 100430.
[26] R.D. Falgout, U.M. Yang, hypre: A Library of high performance preconditioners, in: International Conference On Computational Science, Springer, 2002, pp. 632–641.
[27] C.J. Permann, A.M. Jokisaari, M.R. Tonks, D. Schwen, D.R. Gaston, F. Kong, R. Hiromoto, R.C. Martineau, Scalable feature tracking for finite element meshes demonstrated with a novel phase-field grain subdivision model, Nucl. Technol. (2021) 1–20.
[28] F. Pedregosa, G. Varoquaux, A. Gramfort, V. Michel, B. Thirion, O. Grisel, M. Blondel, P. Prettenhofer, R. Weiss, V. Dubourg, et al., Scikit-learn: Machine learning in Python, J. Mach. Learn. Res. 12 (2011) 2825–2830.
[29] H. Proudhon, Pymicro: A Python package to work with material microstructures and 3d data sets, 2021, https://github.com/heprom/pymicro.
[30] H.J. Rack, G.A. Knorovsky, Assessment of stress-strain data suitable for finite-element elastic–plastic analysis of shipping containers, Technical Report, Sandia National Laboratory, 1978.
[31] E. Fisher, Preparation of alpha uranium single crystals by a grain-coarsening method, JOM 9 (7) (1957) 882–888.
[32] M.R. Tonks, Y. Zhang, A. Butterfield, X.-M. Bai, Development of a grain boundary pinning model that considers particle size distribution using the phase field method, Modelling Simul. Mater. Sci. Eng. 23 (4) (2015) 045009.
[33] D.E. Janney, Metallic Fuels Handbook, Part 1 and Part 2, Technical Report, Idaho National Laboratory, Idaho Falls, ID (United States), 2018.
[34] M.A. Steiner, R.W. Klein, C.A. Calhoun, M. Knezevic, E. Garlea, S.R. Agnew, Efficient rolling texture predictions and texture-sensitive thermomechanical properties of α-uranium foils, J. Nucl. Mater. 495 (2017) 234–243.
[35] F.G. Di Lemma, X. Liu, T.V. Holschuh II, C.P. Folsom, D.J. Murray, F. Teng, C.B. Jensen, Investigation of the microstructure evolution of alpha uranium after in pile transient, J. Nucl. Mater. 542 (2020) 152467.